PERGAMON

Chemical Engineering Science 54 (1999) 5021–5029

Chemical Engineering Science

The boiling slurry reactor: Axial dispersion model

Johannes G. Khinast[a,*], Dan Luss[b], Tiberiu M. Leib[c], Michael P. Harold[d]

[a]*Department of Chemical and Biochemical Engineering, Rutgers University, Piscataway, New Jersey 08854-8058, USA*
[b]*Department of Chemical Engineering, University of Houston, Houston, TX 77204-4792, USA*
[c]*DuPont Engineering, Wilmington, DE 19880-0304, USA*
[d]*DuPont Dacron®, Wilmington, DE 19880-0304, USA*

Abstract

We use a mathematical model that accounts for axial dispersion in both the gas and liquid phases to study the dynamics of a special configuration of a boiling slurry reactor (BSR). It is fed by a nonvolatile liquid reactant, a solvent, and a gaseous reactant and its effluent consists only of a gas. The proposed BSR configuration offers two important advantages over conventional slurry reactors, i.e., complete conversion of the liquid reactant and no need for expensive solid–liquid separation. Additionally, internal cooling devices are not needed since the reactor is cooled by evaporation of the solvent and the liquid products. The results generated by the dispersion model are compared with those of a well-mixed CSTR model. High dispersion — typical of a large diameter commercial scale reactor operating at high superficial gas velocity — leads to a reactor behavior similar to a well-mixed CSTR. Reduced backmixing does not change the qualitative reactor behavior dramatically, although temperature and concentration gradients increase, as expected. At low feed temperatures and very low axial dispersion no steady-state is reached since the reaction does not ignite at the bottom of the column. An increase of the feed temperature will stabilize the operation. A unique feature of this BSR is the possible existence of fill-up and dry-up states at which the reactor volume changes monotonically while the other state variables remain unchanged. The fill-up state will lead to spillover unless the feed and/or initial conditions are properly adjusted.

Keywords: Boiling slurry reactor; Gas–liquid reaction; Reactor dynamics; Axial dispersion model

Nomenclature

a_v	gas–liquid interfacial area per unit liquid volume, 1/m
A_R	reactor cross-section area, m^2
c	molar concentration, kmol/m^3
c_v	heat capacity, kJ/(kmol K)
D	axial dispersion coefficient, m^2/s
D_R	column diameter, m
E	activation energy, kJ/kmol
F	molar flow rate, kmol/m^2 s
F_i^f	feed rate of component i, kmol/s
H	liquid level (expanded bed), m
H_i	Henry's law constant of component i, m^3 bar/kmol
ΔH_r	heat of reaction, kJ/kmol
ΔH_{ad}	heat of adsorption, kJ/kmol
ΔH^v	heat of evaporation at T_R, kJ/kmol
$k_l \cdot a_v$	volumetric mass transfer coefficient, 1/s
k_0	frequency factor, $m^3/(s\ kg_{cat})$
K	gas–liquid equilibrium constant
K_{ad}	adsorption constant, m^3/kmol
N^t	molar phase transfer rate (dissolution, evaporation), kmol/s
P	system pressure, bar
P_v	vapor pressure, bar
r	reaction rate, kmol/(s kg_{cat})
R	universal gas constant, kJ/(kmol K)
t	time, s
T	reactor temperature, K
u_t	superficial velocity, m/s
u_b	terminal rise velocity of the bubble swarm, m/s
$\hat{V}$	molar volume, m^3/kmol
y	mole fraction in the gas phase

* Corresponding author. Fax: 001-732-445-2581.
E-mail address: khinast@sol.rutgers.edu (J.G. Khinast)

0009-2509/99/$ - see front matter
PII: S0009-2509(99)00347-4

Greek letters

β	B/A ratio
λ_{disp}	axial thermal dispersion, kW/m K
v	stoichiometric coefficient
ρ	gas-phase density, kmol/m^3
ρ_s	density of solid catalyst, kg/m^3

Subscripts

g, l, s	gas, liquid, solid phase
R	reference

Superscripts

feed	feed
v	vaporization

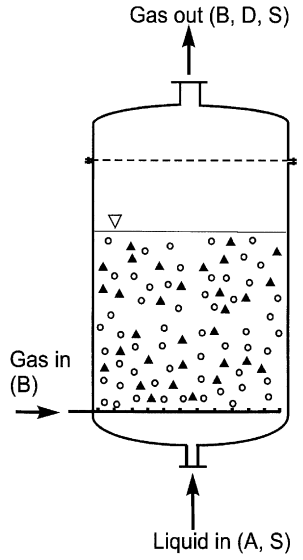

Fig. 1. Schematic of the boiling slurry reactor (BSR).

1. Introduction

Slurry reactors involve catalytic reactions between gaseous and liquid reactants. Recent reviews of these reactors were presented by Shah (1979), Ramachandran and Chaudhari (1983), Gianetto and Silveston (1986), Fan (1989), Hammer et al. (1984), Beenackers and van Swaaij (1986), and Krishna and Ellenberger (1995). In a boiling slurry reactor (BSR) the reaction heat is removed by the evaporation of the reaction mixture. Luyben (1966) noted that a closed-loop control may be needed for stable operation of a BSR. Several important commercial processes such as C_4-alkylation and synthesis of tetraethyl lead and polyethylene utilize a BSR.

We consider here a special configuration of a BSR, where a non-volatile liquid reactant, dissolved in a volatile solvent reacts with a gaseous reactant while the effluent is only gaseous, as illustrated in Fig. 1. Potential applications encompass exothermic gas–liquid reactions for which the reaction products are much more volatile than the liquid reactant, for example the hydrogenation of pyrrole (C_4H_4NH, boiling point 130°C) to pyrrolidine (C_4H_8NH, boiling point 89°C). This configuration has three advantages:

1. The non-volatile liquid reactant is completely converted. This cannot be accomplished in a BSR in which the effluent is a liquid phase.
2. The catalyst remains in the reactor avoiding the expensive catalyst/liquid separation. While internal filtering with recycle may be used when catalyst attrition does not occur, in many applications the catalyst separation from the product is one of the difficult tasks involved in slurry reactor operation.
3. The use of expensive heat exchangers may be eliminated by feeding the reactor with a proper liquid (solvent) with a higher volatility than that of the liquid reactant.

We have previously used a well-mixed reactor model to study the behavioral features of a BSR in which a single exothermic reaction or two exothermic reactions occur. (Khinast, Luss, Lieb & Harold, 1998, 1999). Our studies show that a unique steady-state exists when a single reaction occurs in the BSR, whereas three steady-states may exist for certain sets of parameters when two reactions occur. The case of two consecutive reactions leads to a larger variety of dynamic features than the case of two parallel reactions. An interesting feature of BSR operation is that under certain conditions two types of *pseudo-steady-states* exist in addition to the steady-states. In the first, referred to as a *fill-up state*, the reactor temperature and concentrations of all the species remain virtually constant, while the liquid volume increases monotonically. Clearly, this operation will eventually lead to a spill-over and require shut-down or a proper adjustment of the operating conditions. In the second state, referred to as a *dry-up state*, the liquid volume decreases monotonically, while the other state variables remain unchanged. Eventually, the dry-up state becomes unstable and the system shifts to the closest steady-state, or to a fill-up state if no steady-state exists. We showed that for certain sets of parameters fill-up, dry-up and steady-states coexist and special care has to be taken during reactor start-up in order to avoid shifting to a fill-up state.

Our previous model assumed perfect mixing of the gas and liquid phase. However, gas and liquid mixing in bubble column slurry reactors is intermediate between

plug and well-mixed flow. We extend here our previous work by accounting for axial temperature and concentration gradients in the reactor. While the mixing in large diameter gas–liquid columns is extensive, it may be decreased significantly by use of trays and column packing. Our simulations are intended to provide information on the influence of the dispersion on the start-up, operation and control of the BSR.

2. Convection-Dispersion Model of the BSR

We consider a BSR in which the following single exothermic gas–liquid reaction occurs (Khinast et al., 1998)

$$A_{(l)} + 2B_{(g)} \rightarrow D_{(l)}. \tag{1}$$

The non-volatile organic reactant feed (A) is dissolved in an inert volatile solvent (S). Complete conversion of the non-volatile reactant A has to be obtained at steady-state to avoid its accumulation in the reactor. The gaseous feed is pure B. The catalyst is dispersed in the liquid phase. The heat generated by the exothermic reaction evaporates the liquid product D and the solvent S and preheats the feed to the reaction temperature.

The molar gas and liquid (bubble) phase balances are

$$\frac{\partial c_{i,g}\,\varepsilon_g}{\partial t} = \varepsilon_g D_g \rho \frac{\partial^2 y_i}{\partial x^2} - \frac{\partial u_g c_{i,g}}{\partial x} + N_i^t, \quad i = B, D, S, \tag{2}$$

$$\frac{\partial c_{i,l}\,\varepsilon_l}{\partial t} = \varepsilon_l D_l \frac{\partial^2 c_{i,l}}{\partial x^2} - \frac{\partial u_l c_{i,l}}{\partial x} - N_i^t + v_i r, \quad i = A, B, D, S. \tag{3}$$

In Eqs. (2) and (3) y_i is the mole fraction of species i in the gas phase and $c_{i,l}$ is the molar liquid concentration of species i. We assume that no reactions occur in the gas phase and that the reaction rate in the liquid phase is given by

$$r = \rho_s \varepsilon_s k_0 \exp[-E/RT] \frac{K_{\mathrm{ad}} \cdot c_{A,l}\, c_{B,l}}{1 + K_{\mathrm{ad}}\, c_{A,l}},$$

$$K_{\mathrm{ad}} = K_{\mathrm{ad},0} \exp[-\Delta H_{\mathrm{ad}}/RT]. \tag{4}$$

The sum of the hold-ups add up to one, i.e., $\varepsilon_g + \varepsilon_l + \varepsilon_s = 1$. Hold-ups are assumed to be uniform in the reactor. The holdup of the bubble phase is assumed to be (Saxena, 1995)

$$\varepsilon_g = \frac{u_b^{\mathrm{in}}}{2.5 u_b^{\mathrm{in}} + u_b^t}, \quad u_b^t = 0.23 \text{ m/s}. \tag{5}$$

Saxena (1995) considers u_b^t to be a function of the slurry viscosity, the surface tension and the vapor pressure of the liquid. We assume a constant value for u_b^t and neglect the secondary effect of changing u_b^t. Eq. (5) represents well the effect of the gas superficial velocity, and we neglect the effect of solids on the holdup. This is valid for low solid concentrations but it will break down when approaching high slurry concentrations or dry-out. The solids hold-up is

$$\varepsilon_s = \frac{V_s}{A_R H}, \tag{6}$$

where V_s is the total (constant) catalyst volume, A_R the cross-section area of the reactor and H the variable height of the expanded slurry phase. The local gas–liquid mass-transfer rates N_i^t are

$$N_i^t = \begin{cases} 0, & i = A, \\ V_l k_l a_v \left[c_{B,l} - \dfrac{p_B}{H_B(T)} \right], & i = B, \\ V_l k_l a_v \left[c_{i,l} - \dfrac{c_l y_i}{K_i(T)} \right], & i = D, E. \end{cases} \tag{7}$$

The local convective velocities u_g and u_l in Eqs. (2) and (3) are determined by total volume balances of the gas and liquid phase, i.e., by using the relations

$$\sum_{i=1}^{4} c_{i,l} \hat{V}_i = 1, \tag{8}$$

$$\sum_{i=1}^{3} \frac{c_{i,g} RT}{P} = 1. \tag{9}$$

Multiplication of the individual gas phase mass balances by RT/P and a summation over the three gas-phase species yields a total gas-phase volume balance. Multiplication of the individual liquid-phase mass balances by the molar volume $\hat{V}_i$ and subsequent summation gives the total liquid volume balance, i.e,

$$\frac{\partial u_g}{\partial x} = \sum_{i=1}^{3} \frac{RT(x) N_i^t(x)}{P} + \frac{P}{RT^2} \frac{\partial T}{\partial x}, \tag{10}$$

$$\frac{\partial u_l}{\partial x} = V_i \sum_{i=1}^{4} \hat{V}_i(-N_i^t(x) + v_i r(x)). \tag{11}$$

The $\partial T/\partial x$ term in the first equation Eq. (10) can be safely neglected. The combined energy balance for the solid, gas and liquid phase is

$$\left(\varepsilon_l \sum_i c_{i,l}\, c_{v,i,l} + \varepsilon_g \sum_i c_{i,g}\, c_{v,i,g} + \varepsilon_s\, \rho_s\, c_{p,s} \right) \frac{\partial T}{\partial t} =$$

$$- \Delta H_r(T) \rho_s \varepsilon_s r - \sum_i N_i^t \cdot [\Delta H_i^v(T_R)$$

$$+ (c_{v,i,g} - c_{v,i,l})(T - T_R)]$$

$$- \left(\sum_i F_{i,l} c_{v,i,l} \cdot + \sum_i F_{i,g} c_{v,i,g} \right) \frac{\partial T}{\partial x}$$

$$+ \lambda_{\mathrm{disp}} \frac{\partial^2 T}{\partial x^2}, \quad i = A, B, D, S. \tag{12}$$

A term accounting for the work required to increase the gaseous volume can be safely neglected in the energy balance. In Eq. (12) $F_{i,l}$ and $F_{i,g}$ are the local molar flows, i.e.,

$$F_{i,g} = -\varepsilon_g D_g \rho \frac{\partial y_i}{\partial x} + u_g c_{i,g}, \tag{13}$$

$$F_{i,l} = -\varepsilon_l D_l \frac{\partial c_{i,l}}{\partial x} + u_l c_{i,l}. \tag{14}$$

The reactor pressure is kept constant at P by a PI controller. Boundary conditions are

$x = 0$:

$$c_{i,g} = c_{i,g}^{\text{feed}} + \frac{\varepsilon_g D_g \rho}{u_g^{\text{feed}}} \frac{\partial y_i}{\partial x}, \quad c_{i,l} = c_{i,l}^{\text{feed}} + \frac{\varepsilon_l D_l}{u_l^{\text{feed}}} \frac{\partial c_{i,l}}{\partial x},$$

$$T = T^{\text{feed}} + \lambda_{\text{disp}} \frac{\partial T}{\partial x}, \quad u_g = u_g^{\text{feed}}, \quad u_l = u_l^{\text{feed}}. \tag{15}$$

$x = H$:

$$\frac{\partial c_{i,g}}{\partial x} = \frac{\partial c_{i,l}}{\partial x} = \frac{\partial T}{\partial x} = 0. \tag{16}$$

The initial concentrations and reactor temperature need to be specified. Since the effluent stream may not maintain the liquid level constant, the liquid level depends on several parameters including the feed conditions. Therefore, during reactor start-up the liquid level changes and the model equations are a moving boundary value problem. The rate of change of the liquid level can be determined by integrating the mass transfer and the reactive contribution over the length of the reactor, i.e.,

$$\varepsilon_l \frac{\mathrm{d}H}{\mathrm{d}t} = u_l^{\text{feed}} + \int_0^H \sum_{i=1}^{4} \hat{V}_i(-N_i^t + v_i r)\mathrm{d}x, \quad H = H_0(t=0). \tag{17}$$

The parameter values used in the simulations are reported in Table 1 and the range of parameters applies mostly to the churn-turbulent flow regime ($u_g > 3$–4 cm/s).

In our model we assume that the gas hold-up is based on feed conditions and does not change locally. Other important assumptions are:

1. Instantaneous pressure control.
2. Hydrostatic pressure is negligible.
3. $k_l a_v$ is constant and independent of the components.

The set of model equations consists of 10 dependent, distributed variables (4 liquid concentrations, $c_{i,l}$, 3 gaseous concentrations $c_{i,g}$, the gas and liquid velocities u_g and u_l and the temperature T) and the expanded liquid level H. These variables are described by 8 PDEs (Eqs. (2), (3) and (12)) and 2 boundary value ODEs (Eq. (11)). The liquid level is determined by an integro-differential equation, Eq. (17). Additional algebraic relations are the ideal gas law, the relations for determining the hold-ups and various system parameters (see Appendix A).

The independent variables, which may be controlled are the feed rates and feed temperature, i.e., u_l^{feed}, u_g^{feed}, T^{feed}, and the feed composition. All our computations are based on a liquid feed rate of the reactant A of 0.075 kmol/s. The other feed rates are determined by the feed composition. Unless otherwise mentioned the feed temperature is assumed to be 298 K. We denote the gaseous /liquid feed ratio (B/A-ratio) as

$$\beta = \frac{\nu_A}{\nu_B} \frac{F_{B,g}^{\text{feed}}}{F_{A,l}^{\text{feed}}} = \frac{1}{2} \frac{F_{B,g}^{\text{feed}}}{F_{A,l}^{\text{feed}}}. \tag{18}$$

A β value of unity is the minimum required for complete conversion of the non-volatile reactant A. Clearly, to obtain complete liquid reactant conversion and to avoid its accumulation β should exceed unity. The mole fraction of the reactant in the liquid feed is

$$x = \frac{F_{A,l}^{\text{feed}}}{F_{A,l}^{\text{feed}} + F_{S,l}^{\text{feed}}}. \tag{19}$$

A finite volume method is used to discretize the model equations. Since the liquid level changes dynamically, the model is a moving boundary value problem. We

Table 1
Parameter values used in the simulations

Parameter	Value	Parameter	Value	Parameter	Value
$C_{p,s}$	1.1 kJ/kg/K	$\Delta H_D^v(T_R)$	29 kJ/mol	$\hat{V}_A$	0.073 m^3/kmol
$c_{v,A,l}$	150 kJ/kmol/K	$\Delta H_S^v(T_R)$	44 kJ/mol	$\hat{V}_B$	0.01 m^3/kmol
$c_{v,B,l}$	50 kJ/kmol/K	$\Delta H_B^v(T_R)$	1 kJ/mol	$\hat{V}_C$	0.081 m^3/kmol
$c_{vD,l}$	150 kJ/kmol/K	H_B	60 m^{3}bar/kmol	$\hat{V}_D$	0.018 m^3/kmol
$c_{v,S,l}$	75 kJ/kmol/K	k_0	4×10^7 kmol/(s kg$_{\text{cat}}$)	V_S	0.8 m^3
$c_{v,B,g}$	29 kJ/kmol/K	$K_{\text{ad},0}$	0.1 m^3/kmol	ν_A	-1
$c_{v,D,g}$	40 kJ/kmol/K			ν_B	-2
$c_{v,S,g}$	36 kJ/kmol/K			ν_D	$+1$
D_R	1.5 m^2	$k_l a_v$	0.05 1/s	ν_S	0
E	83 kJ/mol	P	70 bar	ρ_s	1500 kg/m^3
ΔH_{ad}	-21 kJ/mol	T_R	298.0 K		
ΔH_r	-251 kJ/mol	u_b^t	0.23 m/s		

discretize the model equations by specifying finite volumes of equal size, that is, the volume elements change at the same rate if the liquid level changes. In the real system the liquid volume increase or decrease in the column is not uniform. Thus, special care has to be taken in order to account correctly for the fluxes between the different volume elements. In this work between 35 and 70 finite volumes are used, depending on the gradients in the system. The differential-algebraic solver LIMEX (Deuflhard, Hairer & Zugck, 1987) is used to integrate in time the resulting set of ordinary differential equations. Steady-state solutions are computed by using Newton–Raphson and continuation methods. Stability of the solutions is determined by inspection of the linearization spectrum, which is computed by the subroutine RG (EISPACK).

3. Simulation results: High axial dispersion

The axial dispersion coefficients used here for gas, liquid and thermal dispersion are determined from literature correlations for an empty, large diameter, commercial-scale reactor operating with high superficial gas velocity (4.5–9 cm/s). Parameter values are reported in Table 1 and correlations in Eqs. (A.4) and (A.5) in Appendix A. Fig. 2 describes the dependence of the liquid concentration profiles in the reactor on the feed mole fraction x of the limiting liquid reactant A. The parameter β is the molar ratio of gas to liquid reactant and therefore determines the superficial gas velocity. In the case of $\beta = 1.5$ $u_g^{\text{feed}} = 4.5$ cm/s, while for $\beta = 3.0$ $u_g^{\text{feed}} = 9$ cm/s. The simulations show that (with the exception of c_B) the concentration gradients are rather small. The behavior of c_B for $x = 0.23$ is explained by the fact that for this set of operating conditions the reactor is close to the heat generation limit, at which a depletion of A occurs. This leads to a low concentration of A in the top of the column causing small consumption of the dissolved reactant B.

The feed concentration decreases rapidly in the reactor upstream section due to the high dispersion coefficient in the liquid phase. The same trend is observed in the gas phase. Therefore, the BSR behavior is very similar to that of a two-phase CSTR. The gas-phase mole fractions of the gaseous reactant B and the reaction product D are shown in Fig. 3 together with the temperature profile and the liquid net convection velocity u_l. Clearly, in a steady-state u_l approaches zero at the top of the reactor.

The BSR liquid reaction product and solvent have to be completely evaporated during steady-state operation to avoid their accumulation. Thus, a minimum amount of heat has to be released by the reaction. When the reactant feed concentration is below a critical value the heat of the reaction is not sufficient to boil off the liquid and a fill-up state is obtained. Therefore, a heat

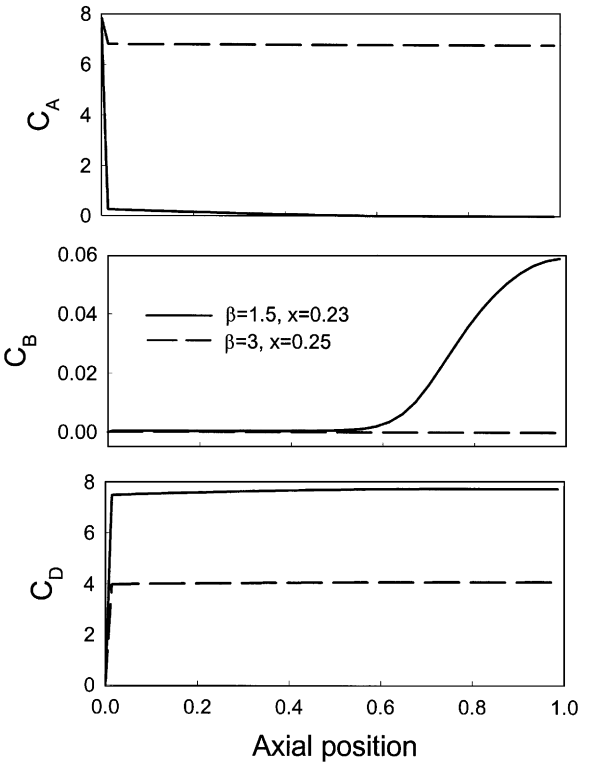

Fig. 2. Steady-state axial concentration profiles in the BSR for two different sets of parameters. In both cases $T^{\text{feed}} = 298$ K.

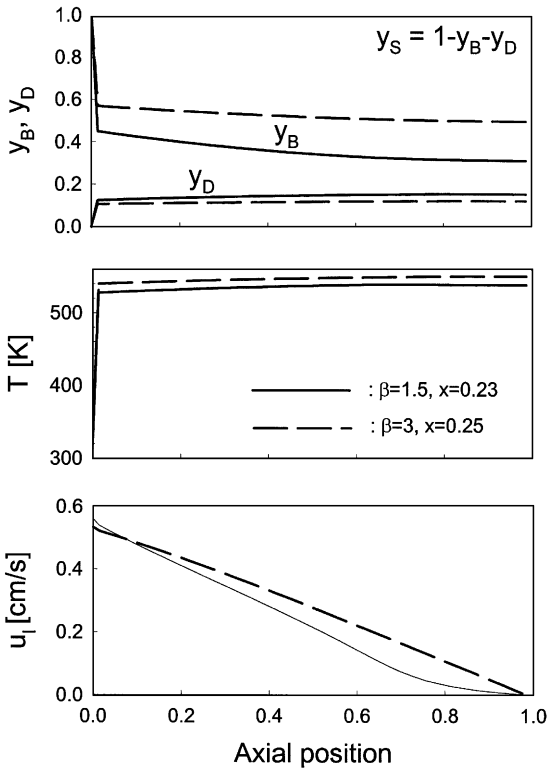

Fig. 3. Steady-state gas-phase concentration, temperature and liquid velocity profiles in the BSR for two different sets of parameters. In both cases $T^{\text{feed}} = 298$ K.

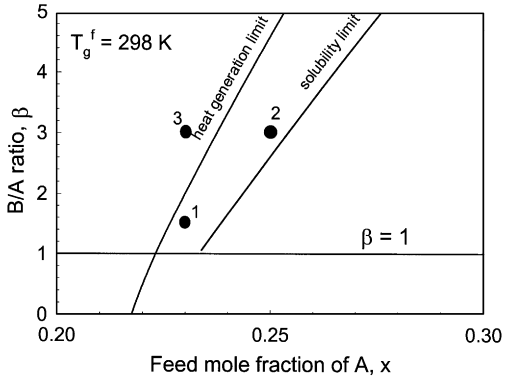

Fig. 4. Feasibility map showing the region of feasible steady-state operation of a BSR. The map was generated by using a well-mixed CSTR model of the BSR (Khinast et al., 1998). The black circles correspond to states depicted in Figs. 2, 3 and 5.

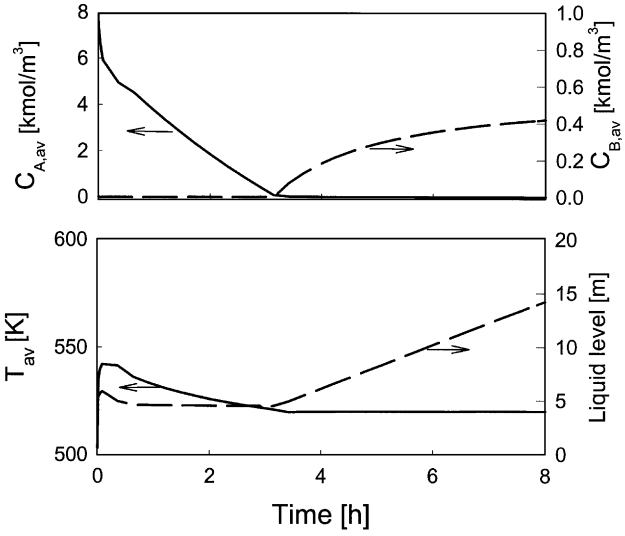

Fig. 5. Shift of the BSR to a fill-up states for $x = 0.23$ and $\beta = 3.0$. The variables are averaged over the reactor height.

generation limit bounds the operating conditions for which steady-state operation is feasible. Similarly, there exists a solubility limit beyond which the concentration of the liquid reactant exceeds its solubility leading to phase separation. Fig. 4 shows these two limiting boundaries, which were computed by use of the well-mixed CSTR-model of the BSR (Khinast et al., 1998). Steady-state operation is feasible only between the heat generation and the solubility limit.

The parameter values of the states shown in Figs. 2 and 3 are denoted in Fig. 4 by two black circles, numbered 1 and 2. Both parameter sets are within the feasible region, but state 1 is closer to the heat generation limit. We showed in our previous work that as the heat generation limit is approached the steady-state liquid volume increases and the liquid concentration c_A decreases. Accordingly, the liquid level in cases 1 and 2 are 5.8 and 4.3 m, respectively. When c_A vanishes, the liquid volume increases without bounds. Fig. 2 shows that for $x = 0.23$ and $\beta = 1.5$ (state 1) the concentration approaches zero in the upper part of the reactor. The concentration of B in that region increases since B is no more consumed by a reaction.

We simulated (Fig. 5) a state in the unfeasible region ($x = 0.23, \beta = 3$), i.e., state 3 in Fig. 4 to check the validity of the map in Fig. 4, which was generated by the CSTR-model, and to confirm the heat generation limit. The average concentrations of the reactants A and B, the average temperature and the liquid level are shown versus time. The reactor is started up at a temperature of $T = 500$ K, with a liquid concentration of 8 kmol/m^3 and an expanded slurry level of 5 m. Initially, the average reactor temperature increases due to the high reaction rate. Gradually, the average concentration of the liquid reactant A decreases and the reactor temperature decreases in turn. After approximately 3 h the initial amount of A is depleted and the heat generated by the reaction is not sufficient to evaporate the products formed and the solvent fed to the reactor. This causes the liquid level to rise leading to an eventual spill over.

Simulations were used to study the impact of the feed conditions on the start up for parameters that correspond to state 2 in Fig. 4, which is within the feasible region. When the reactor is initially cold (298 K) and the feed temperature is 298 K the liquid level increases steadily until spill-over occurs and the desired steady-state is not obtained. The simulations show that for an initial reactor temperature of 298 K a shift to the desired steady-state is obtained only if the feed temperature exceeds 320 K.

A start-up with a cold reactor (298 K) and a feed temperature of 350 K is shown in Fig. 6. Initially, the reactor is cold and completely filled with the solvent. In the first 20 min the reactor temperature and the reactant concentration increase and slowly approach the feed conditions. The liquid level also increases since no evaporation occurs. After 20 min the reactor rapidly ignites, i.e., a high temperature is reached within less than a minute. Following this evaporation leads to a strong decrease of the liquid level. Due to the high reactant concentration the temperature reaches a local maximum and the high reaction rate leads to a fast depletion of the reactant A. After 90 min the reactor begins to slowly shift to a steady-state, which is reached after 4 h.

When the reactor is started with a preheated reactor contents (broken lines) the reaction starts immediately and the initial increase of the liquid level is moderate. Therefore, we conclude that it is beneficial to start up the reactor by preheating its contents. The final steady-state, however, is reached at about the same time as that for the other case.

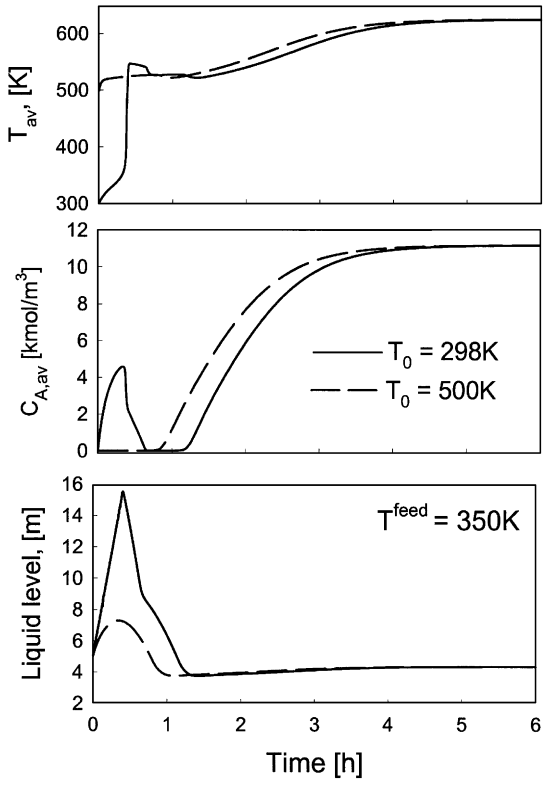

Fig. 6. Dynamic simulation of a reactor start-up. In both cases $T^{feed} = 350$ K and the reactor is initially filled with pure solvent. Initial height of the expanded slurry is 5 m. Solid lines: initial temperature is 298 K. Dashed lines: initial temperature is 500 K.

4. Influence of axial dispersion

Figs. 2 and 3 show that the concentrations in the reactor are rather uniform except for operating conditions close to the heat generation limit. This behavior is caused by the large dispersion coefficients predicted by the correlations of Ramachandran and Chaudhari (1983) and Deckwer, Burckhart and Zoll (1974). For our set of operating conditions and reactor size the dispersion coefficients are approximately $D_l = 0.6\ \mathrm{m^2/s}$, $D_g = 8.5\ \mathrm{m^2/s}$ and $\lambda_{\mathrm{disp}} = 750\ \mathrm{kW/m/K}$. It is therefore not surprising that the axial dispersion model and the well-mixed two-phase CSTR (Khinast et al., 1998) predict very similar behavior as illustrated in Fig. 4.

For certain reactor configurations the extent of liquid and gaseous backmixing may be significantly reduced by perforated trays (Magnussen, Schuhmacher, Rotermund & Hafner, 1978) or packing (Hofmann, 1982). In order to study the influence of reduced backmixing we solved the steady-state solutions for different dispersion coefficients. We assumed that the mass and heat Peclet numbers change in an identical way, i.e., the ratio $Pe_{m,l}/Pe_{m,g}/Pe_h$ is constant. In Fig. 7 the liquid level is plotted versus the factor by which the axial dispersion based on correlations (A.4)–(A.6) (= base-case) is reduced. At first a slight

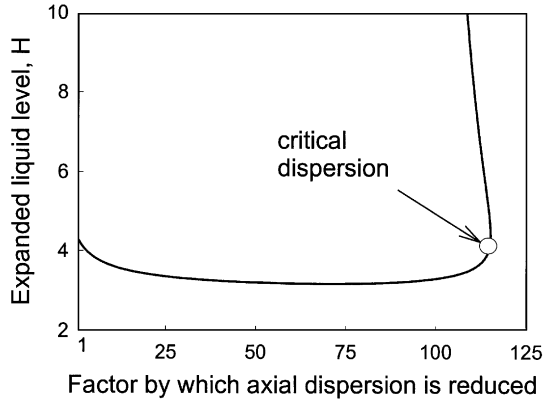

Fig. 7. Liquid level as a function of axial dispersion. $T^{feed} = 298$ K, $x = 0.25$ and $\beta = 3$.

drop in the liquid level occurs. For axial dispersion less than 1/115th of the base-case the liquid level increases sharply. All the steady-states on the vertical branch are unstable. Below the critical axial dispersion limit, the heat dispersion is not sufficient to heat up the cold reactor feed and no steady-state can be reached. Higher feed temperatures can stabilize the reactor operation. We conclude that very low axial dispersion may prevent the reactor from reaching a steady-state at low feed temperatures since the reaction does not ignite in the bottom of the column.

In Fig. 8 the concentration and temperature profiles are compared for the base-case and for a situation where the effective dispersion coefficients are 1/75th and 1/115th of the original ones. The operating conditions are $x = 0.25$ and $\beta = 3$ at a feed temperature of 298 K. Note, that the liquid levels are slightly different in the three cases (see Fig. 7). Significant concentration gradients exist in these cases and the reaction zone is shifted in the down-stream direction as the dispersion coefficient is decreased. For Cases 2 and 3 strong temperature gradients exist. In both cases the maximum temperature, which is reached at the top of the column, significantly exceeds that of the well-mixed case. This may raise safety concerns and it may effect selectivity by inducing undesired side reactions.

The heat generation limit is shown in Fig. 9 for the base-case and for Case 2. We showed (Khinast et al., 1998 Khinast et al., 1999) that the liquid level approaches infinity as the heat generation limit is reached by lowering the feed mole fraction of the liquid reactant A. The same behavior is predicted by the axial dispersion model. Obviously, the heat generation limit is more restrictive in the presence of high axial dispersion. While stable operation is possible for a feed with a mole fraction of $x = 0.235$ in columns with reduced backmixing (Case 2), the corresponding liquid level in a highly mixed column increases with time leading to spill-over. This behavior may be explained by the higher reactant concentration

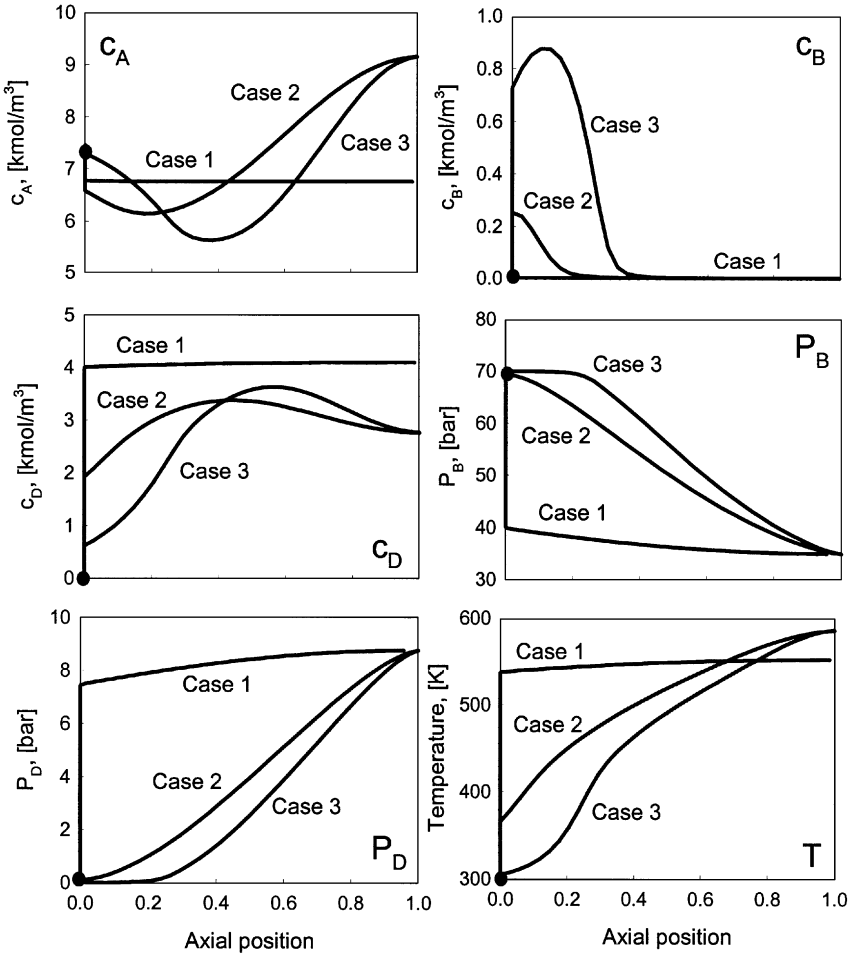

Fig. 8. Comparison of concentration, partial pressures and temperature profiles in the BSR for different axial dispersion coefficients. In all cases $T^{feed} = 298$ K, $x = 0.25$ and $\beta = 3$. The black circle denotes inlet conditions.

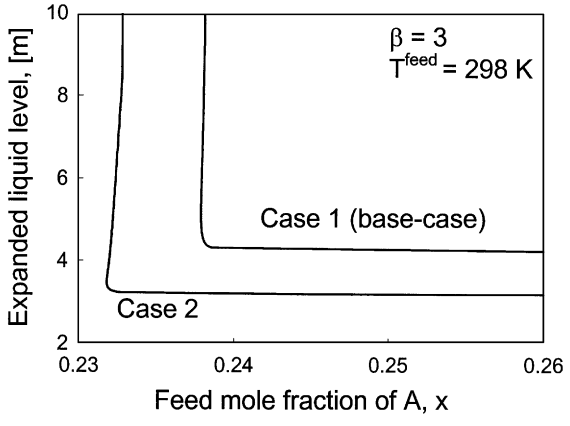

Fig. 9. Dependence of the expanded liquid level on the feed mole fraction x of the liquid reactant for the base-case (Case 1) and Case 2. As H goes to infinity the heat-generation limit is reached.

and temperature in the downstream part of the reactor as the axial dispersion decreases. This, in turn, shifts the reaction quenching (and thus the liquid accumulation) to lower values of the feed reactant A concentration in the feed. We conclude that reduced backmixing increases the feasible operation window, but there is a critical axial dispersion below which a fill-up state is reached instead of the steady-state unless the feed temperature is raised.

5. Conclusions and remarks

The proposed BSR configuration offers several advantages over conventional slurry reactors. It enables complete conversion of the non-volatile liquid reactant, while conventional slurry reactors require a much larger reactor volume to approach complete conversion. Moreover, the BSR does not require an expensive solid–liquid separation, which complicates the operation. Additionally, no internal cooling devices are required since the reactor is cooled by evaporation of the solvent and the liquid products.

In this study we examined the influence of axial dispersion on the start-up and operation of a BSR. Using

literature correlations for the dispersion coefficients in a large diameter reactor operating at high superficial gas velocity the predictions of the dispersion model are similar to those of a CSTR. When the operating conditions are beyond the heat generation limit the axial dispersion model predicts in agreement with the CSTR model a continuous increase of the liquid level (fill-up state).

Trays or packing materials decrease the liquid and gas backmixing. This causes significant temperature and concentration gradients, which may lead to safety problems and reduced selectivity. At the same time it shifts the heat generation limit to lower feed mole fractions of the liquid reactant thus increasing the set of feasible operating conditions. However, for low feed temperatures there is a critical axial dispersion level, below which no operation is possible.

The existence of dry-up and fill-up states is a unique feature of the BSR. Their existence can increase significantly the sensitivity of the start-up procedure on the initial conditions. Careful reactor start-up is required and it is beneficial to preheat the reactor in order to avoid initial liquid accumulation.

Appendix A

The equilibrium constants K_i are given by

$$K_i = \frac{P_{v,i}}{P}. \tag{A.1}$$

The vapor pressures P_v of the components D and S are

$$\log(P_{v,D}) = 4.791 - 1717.4/T \tag{A.2}$$

$$\ln(P_{v,S}) = 5.4 + (1-z)^{-1} \left(-7.765z + 1.458z^{1.5} - 2.776z^3 - 1.233z^6 \right),$$

$$z = 1 - T/647.3 \tag{A.3}$$

The gas- and liquid-phase dispersion coefficient are computed by the relations given by Ramachandran and Chaudhari (1983):

$$D_l = 0.68(u_g^{\text{feed}})^{0.3} D_R^{1.4}, \tag{A.4}$$

$$D_g = 50\left(\frac{u_g^{\text{feed}}}{\varepsilon_g}\right)^3 D_R^{1.5}, \tag{A.5}$$

where D_R is the column diameter in m and the superficial velocities are in m/s. Note, that we use dispersion coefficients based on inlet conditions. The thermal dispersion coefficients are given by Deckwer et al. (1974) by equating the liquid mass and the thermal dispersion Pe numbers:

$$\lambda_{\text{disp}} = D_l \, c_{v,m,l} \rho_l, \tag{A.6}$$

where $c_{v,m,l}$ and ρ_l are the heat capacity and the density of the liquid mixture. Note, that we calculate dispersion coefficients based on reactor inlet conditions.

References

Beenackers, A. A. C. M., & van Swaaij, W. P. H. (1986). Chemical Reactor Design and Technology. In H. I. DeLasa, *NATO advanced study institute series* (pp. 463–538). Dordrecht: Martinus Nijhoff.

Deckwer, W.D., Burckhart, R., & Zoll, G., (1974). Mixing and mass transfer in tall bubble columns. *Chemical Engineering Science*, 29, 2177.

Deuflhard, P., Hairer, E., & Zugck, J. (1987). One-step and extrapolation methods for differential-algebraic systems. *Numerical Mathematics*, *51*, 1.

Fan, L. S. (1989). *Gas–liquid–solid fluidization engineering*. Boston: Butterworths.

Gianetto, A., & Silveston, O. L. (1986). *Multiphase chemical reactors*. Washington DC: Hemisphere.

Hammer, H., Kusters, U., Schrag, H. J., Soemarno, A., Sahabi, U., Schonau, H., & Napp, U. (1984). In L. K. Doraiswamy, *Recent advances in the engineering analysis of chemically reacting systems* (pp. 379–395). New Delhi: Wiley India.

Hofmann, H. (1982). Packed upflow bubble columns. *Chemie. Ingenieur. Technik*, *54*(10), 865–876.

Khinast, J., Luss, D., Leib, T. M., & Harold, M. P. (1998). The boiling slurry reactor: Feasible operation and stability. *A.I.Ch.E. Journal*, *44*(8), 1868.

Khinast, J., Luss, D., Leib, T.M., & Harold, M.P. (1999). Impact of an undesired reaction on a boiling slurry reactor. *Chemical Engineering Science*, *54* (13–14), 2295.

Krishna, R., & Ellenberger, J. (1995). A unified approach to the scale-up of "fluidized" multiphase reactors. *Transactions of the Institution of Chemical Engineers*, *73*(A), 217–221.

Luyben, W. L. (1966). Stability of autorefrigerated chemical reactors. *A.I.Ch.E.Journal*, *12*(4), 662–668.

Magnussen, P., Schuhmacher, V., Rotermund, G. W., & Hafner, F. (1978). *Chemie-Ingenieur-Technik.*, *50*, 811.

Ramachandran, P. A., & Chaudhari, R. V. (1983). *Three phase catalytic reactor*. New York: Gordon and Breach.

Saxena, S. C. (1995). Bubble column reactors and Fischer–Tropsch synthesis. *Catalytic Reviews in Science Engineering*, *37*(2), 227–309.

Shah, Y. T. (1979). *Gas–liquid–solid reactor design*. New York: McGraw-Hill.